plaque burden: from the Rule Out Myocardial Infarction using Computer Assisted Tomography (ROMICAT) trial. Am Heart J 2009;158: 562–8.
[18] Otto CM, Lind BK, Kitzman DW, Gersh BJ, Siscovick DS. Association of aortic-valve sclerosis with cardiovascular mortality and morbidity in the elderly. N Engl J Med 1999;341:142–7.
[19] Kohsaka S, Jin Z, Rundek T, et al. Impact of mitral annular calcification on cardiovascular events in a multiethnic community: the Northern Manhattan Study. JACC Cardiovasc Imaging 2008;1:617–23.
[20] Santos RD, Rumberger JA, Budoff MJ, et al. Thoracic aorta calcification detected by electron beam tomography predicts all-cause mortality. Atherosclerosis 2010;209:131–5.

International Journal of Cardiology xxx (2011) xxx–xxx

Contents lists available at ScienceDirect

International Journal of Cardiology

journal homepage: www.elsevier.com/locate/ijcard

Underestimation of aortic valve area in calcified aortic valve disease: Effects of left ventricular outflow tract ellipticity

Hiroto Utsunomiya [a], Hideya Yamamoto [a,*], Jun Horiguchi [b], Eiji Kunita [a], Takenori Okada [a], Ryo Yamazato [a], Takayuki Hidaka [a], Yasuki Kihara [a]

[a] Department of Cardiovascular Medicine, Hiroshima University Graduate School of Biomedical Sciences, Hiroshima, Japan
[b] Department of Clinical Radiology, Hiroshima University Hospital, Hiroshima, Japan

ARTICLE INFO

Article history:
Received 13 August 2010
Received in revised form 11 December 2010
Accepted 20 December 2010
Available online xxxx

Keywords:
Aortic valve area
Continuity equation
Ellipticity
Left ventricular outflow tract area
Multidetector computed tomography

ABSTRACT

Background: The aortic valve area (AVA) is usually calculated using the continuity equation (CE) in which the left ventricular outflow tract (LVOT) area is estimated assuming circular geometry. We sought to evaluate the LVOT ellipticity with 64-multidetector computed tomography (MDCT) and to assess the impact of LVOT ellipticity on the evaluation of CE-based AVA in patients with calcified aortic valves.

Methods: We prospectively studied 110 patients with calcified aortic valves including 54 aortic stenosis (AS) with both 64-MDCT and transthoracic echocardiography. Double oblique transversal images for planimetry of the aortic valve and LVOT were obtained during the midsystolic phase. The short and long-axis diameters of the planimetered LVOT were measured.

Results: The MDCT planimetered LVOT area was underestimated by the diameter-derived ($\pi \times r^2$) LVOT area using echocardiography (444 ± 70 mm^2 versus 369 ± 63 mm^2; $p<0.001$). The mean difference in AVA values calculated using the CE and planimetry was 0.43 ± 0.23 cm^2 and mean measurement error of CE-based AVA was 18%. When the CE-based AVA was corrected using the MDCT planimetered LVOT area, the measurement error decreased from 28 ± 5 to 5 ± 2% in patients with severe aortic stenosis (AVA<1.0 cm^2), whereas from 16 ± 5 to 3 ± 6% in others.

Conclusion: Ellipticity of LVOT is associated with underestimation of AVA measurements using the CE. CE-based AVA corrected with MDCT planimetered LVOT area is useful especially in severe AS.

1. Introduction

To assess the severity of aortic stenosis (AS) using Doppler echocardiography, aortic valve area (AVA) is usually estimated using the CE [1]: $AVA = LVOT\ area \times (VTI_{LVOT}/VTI_{AV})$, where *LVOT area* is the cross-sectional area of the left ventricular outflow tract (LVOT) calculated from a measured LVOT diameter, with the assumption that the LVOT is circular. *VTI* is the velocity–time integral measured from Doppler tracings at the LVOT and aortic valve.

Although good correlation between planimetry and CE-based measurements of AVA has been obtained, planimetric AVA measurements always yield greater AVA values than those calculated using the CE [2]. Multidetector computed tomography (MDCT) can provide an accurate and noninvasive imaging technique, not only for the coronary artery, but also for aortic valve planimetry [3] and geometry including the aortic annulus and LVOT [4]. Several studies using 64-MDCT have demonstrated that the LVOT is elliptical rather than round in shape [5,6]. It has also been found that the assumption of circular geometry in calculating the LVOT area using echocardiography and the CE ($\pi \times r^2$) consistently underestimates the actual LVOT area measured by MDCT in a wide variety of pathological conditions [5,6]. However, these investigations have not been sufficiently validated in patients with calcified aortic valve disease. Thus, we sought to extensively evaluate LVOT ellipticity with 64-MDCT and to assess the impact of LVOT ellipticity on the evaluation of AVA using echocardiography.

2. Methods

2.1. Study population

We prospectively recruited 163 consecutive patients referred for echocardiography and scheduled for subsequent MDCT angiography. Both examinations were performed within 1 week. Exclusion criteria included: grade >2/4 aortic regurgitation; bicuspid aortic valve; previous surgery of the aortic valve or the ascending aorta; reduced LV contraction (LV ejection fraction <50%); and LVOT obstruction (LVOT flow velocity >2 m/s). A final number of 110 patients with aortic valve calcification were enrolled in the study. BMI was used as a marker of obesity: BMI (kg/m^2) = weight (kg)/height (m)^2. The body surface area (BSA) was calculated as follows: BSA (m^2) = $88.83 \times$ height (cm)$^{0.663} \times$ weight (kg)$^{0.444}$. The study protocol was approved for use by the Human Studies Subcommittee of Hiroshima University Graduate School of Biomedical Sciences. Prior written informed consent was obtained from all participants.

* Corresponding author. Department of Cardiovascular Medicine, Hiroshima University Graduate School of Biomedical Sciences, 1-2-3 Kasumi, Minami-ku, Hiroshima 734-8551, Japan. Tel.: +81 82 257 5540; fax: +81 82 257 1569.
E-mail address: hideyayama@hiroshima-u.ac.jp (H. Yamamoto).

0167-5273/$ – see front matter
doi:10.1016/j.ijcard.2010.12.071

Please cite this article as: Utsunomiya H, et al, Underestimation of aortic valve area in calcified aortic valve disease: Effects of left ventricular outflow tract ellipticity, Int J Cardiol (2011), doi:10.1016/j.ijcard.2010.12.071

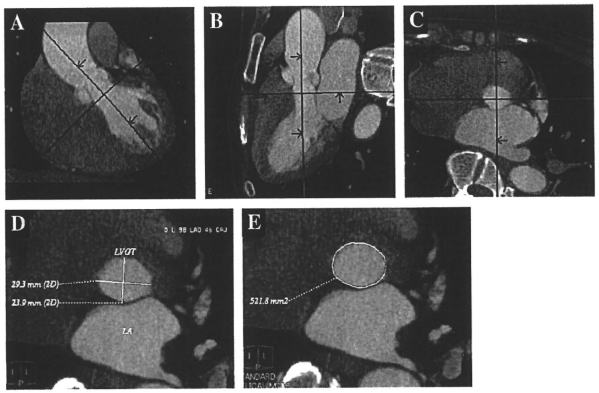

Fig. 1. The left coronal view (A) and the single oblique sagittal view (B) were reconstructed to measure the planimetric AVA. For the planimetry of the LVOT, the double oblique transversal view of the LVOT was reconstructed immediately below the aortic valve parallel to the plane used for measurement of the AVA (C). The short-axis image of the LVOT shows a clearly evident oval shape (D). The directly measured LVOT area is acquired by planimetry (E). AVA = aortic valve area; LVOT = left ventricular outflow tract; MDCT = multidetector computed tomography.

2.2. Multidetector computed tomography

The MDCT examinations were performed with a 64-MDCT scanner (LightSpeed VCT, GE Healthcare, Waukesha, WI). For the MDCT coronary angiogram, a collimation of 64 × 0.625 mm and a gantry rotation time of 350 ms were used. Standard scanning parameters were set to 120 kV and 600 mA. Following a test bolus examination to determine the start of the contrast-enhanced scan, a retrospective ECG-gated CT angiography was performed using a helical mode during an inspiratory breath-hold. The mean radiation dose for the group was 14.4 mSv. To avoid motion artifacts, all patients with an initial heart rate ≥60 beats/min were given an oral β-blocker (metoprolol 40 mg) to achieve a target heart rate of 50–60 bpm. A body weight-adjusted volume (0.6–0.7 mL/kg) of nonionic contrast material (Iopamiron 370, Bayer Healthcare, Berlin, Germany) was administrated via the antecubital vein over a period of 10 seconds, followed by 25 ml of saline solution injected at 5.0 mL/s. Image reconstruction was retrospectively gated to ECG. The dataset of the contrast-enhanced scan was reconstructed at every 5% of the R–R interval. Axial datasets were then transferred to a remote computer workstation (Advantage Workstation Ver.4.2, GE Healthcare) for post-processing and subsequent image analysis.

2.3. Image analysis

For the purpose of LVOT and aortic valve planimetry, we determined a plane perpendicular to the LVOT and aortic root using the double oblique method [3,4]. Namely, a left coronal and a single oblique sagittal view through the LVOT and aortic valve were reconstructed (Fig. 1A and B). Then, maximum effort was made to correctly orientate both planes by simultaneously reviewing the reconstructed double oblique transversal view of the aortic leaflet tips. Planimetry of the aortic valve was performed during the midsystolic phase, which provided the largest AVA with the fewest artifacts [7]. Likewise, planimetry of the LVOT cross-sectional area was performed just beneath the aortic annulus in a plane perpendicular to the LVOT long axis in the same phase as that used for the measurement of the AVA (Fig. 1C).

For the purpose of measurement of LVOT ellipticity, we measured the short- (a) and long- (b) axis diameters of the planimetered LVOT view. The ellipsoidal-estimated LVOT area was calculated using the equation for an ellipse ($\pi \times a/2 \times b/2$). Furthermore, the ellipticity index was calculated using the equation $1-(a/b)$ to quantify the degree of deviation of the LVOT shape from a perfect circle (Fig. 1D and E). Using this index, an ellipticity index of zero represents a perfect circle with a higher index describing a more elliptical geometry.

Intra- and interobserver variability of MDCT measurements were calculated as the coefficient of variation in 10 randomly selected subjects. Intraobserver reproducibility was assessed for a single observer on two separate occasions and interobserver variability was performed by two independent experienced investigators.

2.4. Echocardiography

Comprehensive echocardiograms were performed by an experienced sonographer using high-quality commercially available ultrasound systems (GE Healthcare Vivid 7, Milwaukee, WI) equipped with S4 transducer. Images were obtained in the parasternal (long- and short axis) and apical views. LV volume and ejection fraction were calculated from apical 2- and 4-chamber views using the biplane Simpson's rule according to the recommendation of the American Society of Echocardiography [8]. LV mass was measured using M-mode echocardiography [9]. The LVOT diameter was measured during midsystole immediately below the aortic annulus from the parasternal long-axis view [8]. Using πr^2, the diameter-derived LVOT area was calculated. For the calculation of the CE-based AVA, VTI at the LVOT and the aortic

Table 1
Clinical characteristics, echocardiographic findings and MDCT measurements (n = 110).

Characteristics	Findings
Clinical data	
Age (years)	70 ± 9
Male (%)	47
Height (cm)	157 ± 10
Weight (kg)	58 ± 11
Body mass index (kg/m^2)	23.5 ± 3.1
Body surface area (m^2)	1.58 ± 0.19
Echocardiographic data	
Peak aortic valve velocity (m/s)	2.3 ± 1.3
CE-based AVA (cm^2)	1.99 ± 0.84
Mild AS, n (%)	22 (20)
Moderate AS, n (%)	12 (11)
Severe AS, n (%)	20 (18)
LV end-diastolic volume (ml)	84 ± 24
LV end-systolic volume (ml)	26 ± 13
LV ejection fraction (%)	69 ± 9
Interventricular septal wall thickness (mm)	10.6 ± 2.0
LV posterior wall thickness (mm)	10.4 ± 1.6
LV mass index (g/m^2)	101 ± 31
LVOT diameter (mm)	21.6 ± 1.8
MDCT measurements	
MDCT planimetered AVA (cm^2)	2.47 ± 1.03
LVOT short axis diameter (mm)	21.3 ± 1.9
LVOT long-axis diameter (mm)	26.8 ± 2.4
Ellipsoidal-estimated LVOT area (mm^2)	449 ± 72
MDCT planimetered LVOT area (mm^2)	444 ± 70
Ellipticity index	0.20 ± 0.04

Values are expressed as mean ± SD or number (percentage).
AVA = aortic valve area; AS = aortic stenosis; CE = continuity equation; LVOT = left ventricular outflow tract; MDCT = multidetector computed tomography.

Please cite this article as: Utsunomiya H, et al, Underestimation of aortic valve area in calcified aortic valve disease: Effects of left ventricular outflow tract ellipticity, Int J Cardiol (2011), doi:10.1016/j.ijcard.2010.12.071

Table 2
Correlation of the MDCT planimetered LVOT area and the ellipticity index with demographic and echocardiographic variables.

Variables	LVOT area		Ellipticity index	
	Spearman's R	p	Spearman's R	p
Age	−0.34	<0.001	0.04	0.69
Height	0.63	<0.001	−0.17	0.07
Weight	0.51	<0.001	−0.08	0.39
Body surface area	0.57	<0.001	−0.13	0.17
Systolic blood pressure	0.09	0.63	−0.15	0.23
Peak aortic valve velocity	−0.13	0.19	0.39	<0.001
LV end-diastolic volume	0.41	<0.001	0.04	0.68
LV end-systolic volume	0.52	<0.001	0.01	0.91
Interventricular septal wall thickness	0.18	0.07	0.31	0.001
LV mass index	0.13	0.24	0.31	0.001
LVOT diameter	0.81	<0.001	−0.21	0.03

Abbreviations are as detailed in Table 1.

valve were recorded using pulse Doppler from the apical 5-chamber view. Peak aortic valve velocity and mean transaortic pressure gradient were measured in multiple views (apical long axis, apical 5-chamber and right parasternal) and the maximum values were used [10]. AS was defined as CE-based AVA<2.0 cm^2. Classification of AS was based on the recommendation of the American Society of Echocardiography (mild: aortic valve restriction with AVA>1.5 cm^2, moderate: AVA 1.0 to 1.5 cm^2, and severe: AVA<1.0 cm^2) [1].

2.5. Statistical analysis

All measurements were expressed as mean ± SD. The unpaired *t* test or Mann–Whitney *U*-test was used to compare continuous variables with or without normal distribution, respectively. The MDCT planimetered LVOT area was compared with the diameter-derived LVOT area and ellipsoidal-estimated LVOT area using a paired *t* test and Pearson's correlation coefficient *r*. Agreements between methods (MDCT planimetered LVOT area versus diameter-derived LVOT area; MDCT planimetered LVOT area versus ellipsoidal-estimated LVOT area; and CE-based AVA versus MDCT planimetered AVA) were tested using Bland–Altman analyses and plotted with lines representing the mean ± 2SD. Relationships between LVOT measurements and patients' demographic parameters were assessed using Spearman rank correlations. A probability value of $p<0.05$ was considered significant. All statistical analyses were performed using SPSS 12.0 (SPSS Inc, Chicago, IL).

3. Results

3.1. Relationships between LVOT measurements and demographic variables

Table 1 shows the clinical characteristics, echocardiographic findings and CT measurements of the study population. The mean CE-based

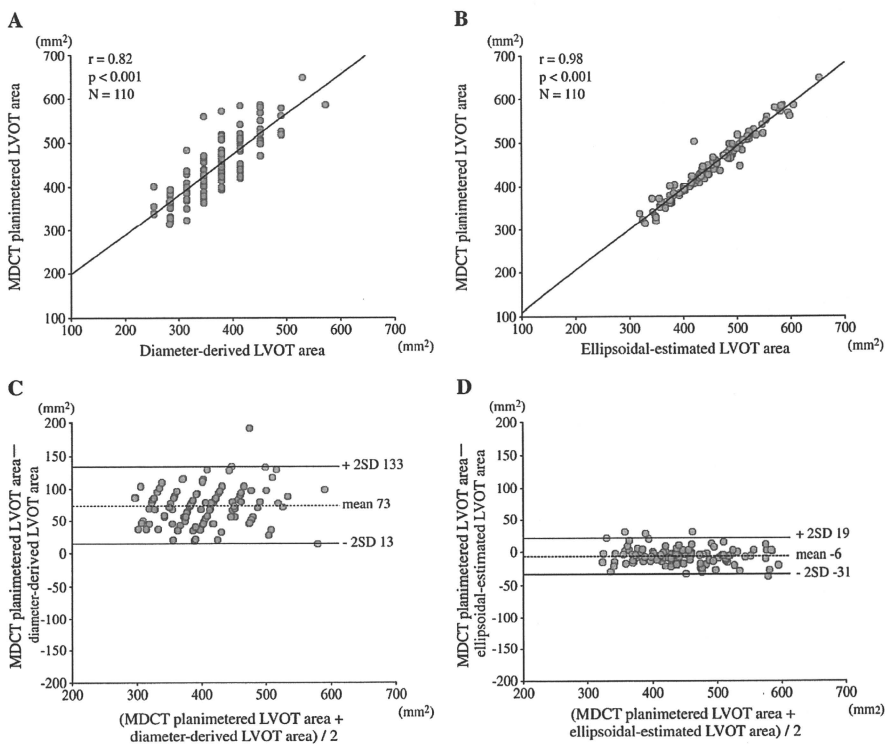

Fig. 2. Scatterplot of correlation between MDCT planimetered LVOT area and diameter-derived LVOT area calculated using echocardiography (A) and that between the MDCT planimetered LVOT area and the ellipsoidal-estimated LVOT area (B). Bland–Altman plot analysis shows that the MDCT planimetered LVOT area has a poor agreement with the diameter-derived LVOT area (C), whereas has a good agreement with the ellipsoidal-estimated LVOT area (D). Abbreviations are as detailed in Fig. 1.

Please cite this article as: Utsunomiya H, et al, Underestimation of aortic valve area in calcified aortic valve disease: Effects of left ventricular outflow tract ellipticity, Int J Cardiol (2011), doi:10.1016/j.ijcard.2010.12.071

AVA value was 1.99 ± 0.84 cm^2, including 54 patients with AS (mild, n = 22; moderate, n = 12; severe, n = 20). Diameters of the ascending aorta measured by MDCT ranged from 30 to 44 mm.

Table 2 shows the correlation between the MDCT planimetered LVOT area and the ellipticity index with the patients' demographic and echocardiographic variables. The LVOT area was the parameter most highly correlated with height (r = 0.63; p<0.001), followed by the BSA (r = 0.57; p<0.001). These correlations remained robust after adjustment for age. After indexing for BSA, the LVOT area was found to be similar in both genders (277 ± 45 mm^2/m^2 in men versus 275 ± 30 mm^2/m^2 in women; p = 0.43). In addition, the ellipticity index did not differ significantly between both genders (0.20 ± 0.05 in men versus 0.21 ± 0.04 in women; p = 0.40).

3.2. Planimetered LVOT area and ellipticity in patients with calcified aortic valve disease

The mean difference between the short- and long-axis LVOT diameters was 5.5 ± 1.6 mm, and the ellipticity index was 0.20 ± 0.04. The Pearson correlation coefficient between LVOT diameter values measured using echocardiography and MDCT was 0.78 (p<0.001). The LVOT diameter measured using echocardiography (*i.e.* anteroposterior diameter) corresponded approximately to the short-axis LVOT diameter (mean difference, 0.2 ± 0.3 mm; p = 0.11). This led to the discrepancy in LVOT area measurements between MDCT planimetry and echocardiography. The actual LVOT cross-sectional area was significantly underestimated using echocardiographic diameter-derived LVOT area measurement (444 ± 70 mm^2 versus 369 ± 63 mm^2; p<0.001).

The MDCT planimetered LVOT area correlated more closely with the ellipsoidal-estimated LVOT area than with the diameter-derived LVOT area (r = 0.98 versus 0.82) (Fig. 2A and B). In addition, Bland–Altman analyses were used to test the agreement between diameter-derived LVOT areas versus MDCT planimetered LVOT areas (Fig. 2C), and ellipsoidal-estimated LVOT areas versus MDCT planimetered LVOT areas (Fig. 2D). The ellipsoidal-estimated LVOT area had narrower limits of agreement and less bias. The mean differences between the MDCT planimetered LVOT area and the diameter-derived LVOT area, and ellipsoidal-estimated LVOT area were 73 ± 30 mm^2 and −6 ± 12 mm^2, respectively.

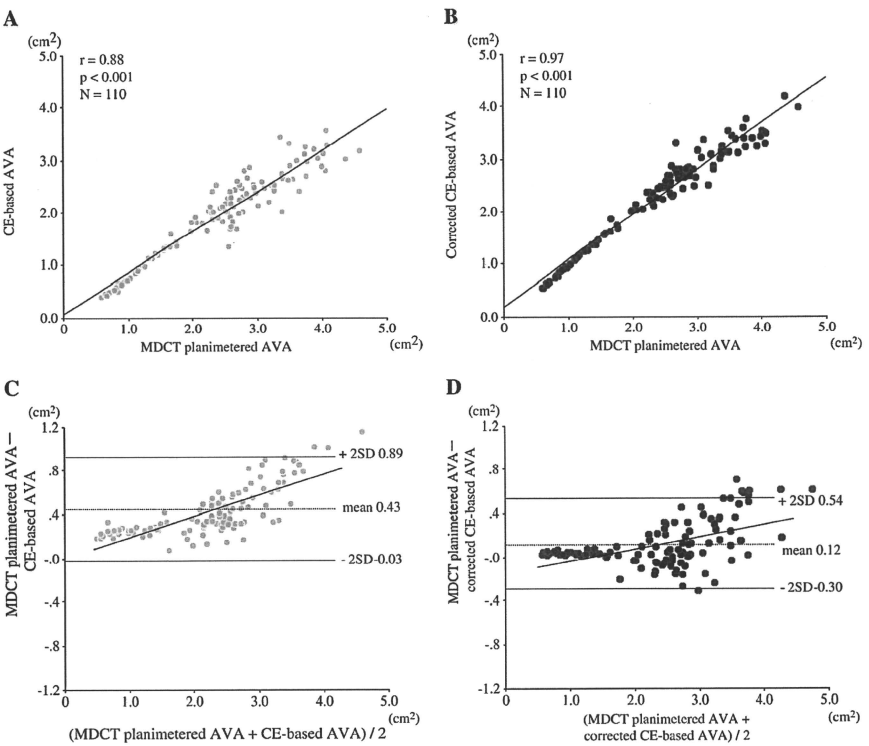

Fig. 3. Scatterplot of the correlation between the MDCT planimetered AVA and the continuity equation (CE)-based AVA calculated using echocardiography (A) and that between the MDCT planimetered AVA and the CE-based AVA corrected by using the MDCT planimetered LVOT area in the calculation (B). Bland–Altman plot analysis shows that the MDCT planimetered AVA has a poor agreement with the CE-based AVA (C), whereas has a good agreement with the CE-based AVA corrected using MDCT planimetered LVOT area (D). Bold lines represent regression lines (C; r = 0.78, p<0.001, D; r = 0.49, p<0.001). Abbreviations are as detailed in Fig. 1.

Please cite this article as: Utsunomiya H, et al, Underestimation of aortic valve area in calcified aortic valve disease: Effects of left ventricular outflow tract ellipticity, Int J Cardiol (2011), doi:10.1016/j.ijcard.2010.12.071

The mean coefficients of variations, within and across observers, were within an acceptable range for the MDCT planimetered LVOT area (2.7% and 4.4%, respectively) and the ellipticity index (3.1% and 5.3%, respectively).

3.3. Impact of LVOT ellipticity on the AVA measurements

Using CE-based calculations, the AVA was significantly underestimated relative to the MDCT planimetered AVA (1.99 ± 0.84 cm^2 versus 2.47 ± 1.03 cm^2, $p<0.001$). When the CE was corrected using the MDCT planimetered LVOT area (*i.e.* the MDCT planimetered LVOT area was substituted into the CE in place of the diameter-derived LVOT area), the measured values were still significantly smaller than those obtained using planimetry (2.34 ± 0.92 cm^2 versus 2.47 ± 1.03 cm^2, $p<0.001$), but the difference between both measurements of AVA significantly decreased ($p<0.001$). The correlation coefficient improved from 0.88 to 0.97 (Fig. 3A and B). Similarly, Bland–Altman analyses revealed that there was better agreement between CE-based AVAs corrected with directly measured LVOT areas and MDCT planimetered AVAs, than between CE-based AVAs and MDCT planimetered AVAs (Fig. 3C and D). The mean differences between the MDCT planimetered AVA and the CE-based AVA, and the corrected CE-based AVA were 0.43 ± 0.23 cm^2 and 0.12 ± 0.21 cm^2, respectively. In patients with severe AS ($n=20$), 6 patients were reclassified as moderate after CE correction using the MDCT planimetered LVOT area.

Fig. 4A depicts the relationship between the measurement error of CE-based AVA and MDCT planimetered AVA. On average, the MDCT planimetered AVA measurements indicated that the CE-based AVA calculations underestimated values by 18 ± 7%. Notably, patients with severe AS (AVA<1.0 cm^2) had a larger measurement error than others (28 ± 5% versus 16 ± 5%, $p<0.001$). By correcting the impact of underestimation of LVOT area on the AVA values, the measurement error of CE-based AVA significantly decreased and did not differ between severe AS group and others (5 ± 2% versus 3 ± 6%, $p=0.36$; Fig. 4B). Percent changes in measurement error were more improved in patients with severe AS than in others (23 ± 3% versus 13 ± 7%, $p<0.001$).

Fig. 5 shows the echocardiographic and CT findings in a representative case with severe AS. When the CE was corrected by inclusion of the MDCT planimetered LVOT area, the measurement error of the CE-based AVA decreased from 39% to 8%.

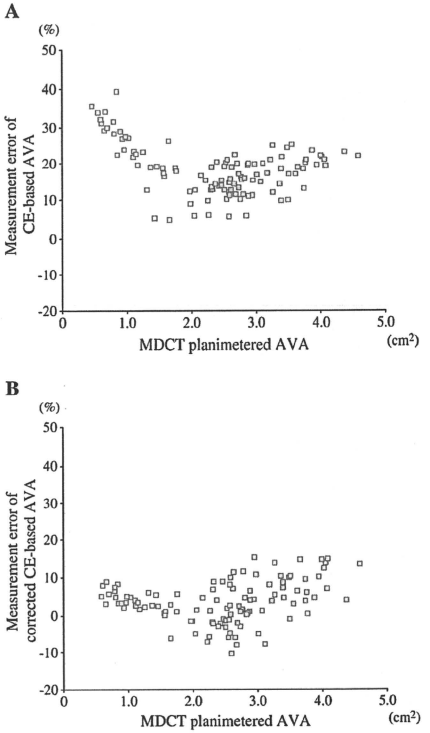

Fig. 4. Scatterplot of relationship between measurement error of CE-based AVA and MDCT planimetered AVA (A) and that between measurement error of corrected CE-based AVA and MDCT planimetered AVA (B).

4. Discussion

In the present study, we demonstrated the following. 1) The MDCT planimetered LVOT area was positively correlated with body size regardless of gender, whereas the ellipticity index was independent of age, gender and body size. 2) In patients with calcified aortic valves without LVOT obstruction, the anatomy of the LVOT cross-sectional area had an elliptical shape during the midsystolic phase. 3) The diameter-derived LVOT area was smaller than MDCT planimetered LVOT area, resulting in the underestimation of AVA measurements using the CE. 4) The corrected CE-based AVA using the MDCT planimetered LVOT area improved the measurement error of CE-based AVA, especially in patients with severe AS.

4.1. Anatomical observation of LVOT area and geometry assessed by MDCT

Degenerative AS is the most common valvular disease related to an atherosclerotic process [11], valvular inflammation and metabolic disorder [12]. Currently, the American Society of Echocardiography recommends that effective AVA based on the CE be used as the standard method for quantitative evaluation of AS [1]. In the CE, the LVOT area component of the equation is not measured directly but estimated using the LVOT diameter from a parasternal long-axis view (corresponding to anteroposterior view) assuming a circular geometry. However, in the present study, the MDCT planimetered LVOT area was more closely related to the ellipsoidal-estimated LVOT area than the diameter-derived LVOT area, indicating that the cross section of the LVOT is oval during the midsystolic phase. Furthermore, echocardiographically derived anteroposterior measurements of LVOT diameters correspond approximately to the minor diameters of an elliptical LVOT, resulting in significant underestimations of the actual cross-sectional LVOT areas. These findings are in agreement with those detailed in the most recent report where 64-MDCT was used, but the study population was limited to patients with severe AS referred for transcatheter aortic valve implantations (TAVI) [13].

4.2. LVOT ellipticity and CE-based measurements of AVA

Our results showed that CE-based AVA generally underestimated MDCT planimetered AVA, with a mean measurement error of 18%. Gilon et al. reported that the discrepancy between both measurements of AVA ranged from 10% to 30% and varied prominently with valve shape [14]. Other explanations about the observed discrepancy

Please cite this article as: Utsunomiya H, et al, Underestimation of aortic valve area in calcified aortic valve disease: Effects of left ventricular outflow tract ellipticity, Int J Cardiol (2011), doi:10.1016/j.ijcard.2010.12.071

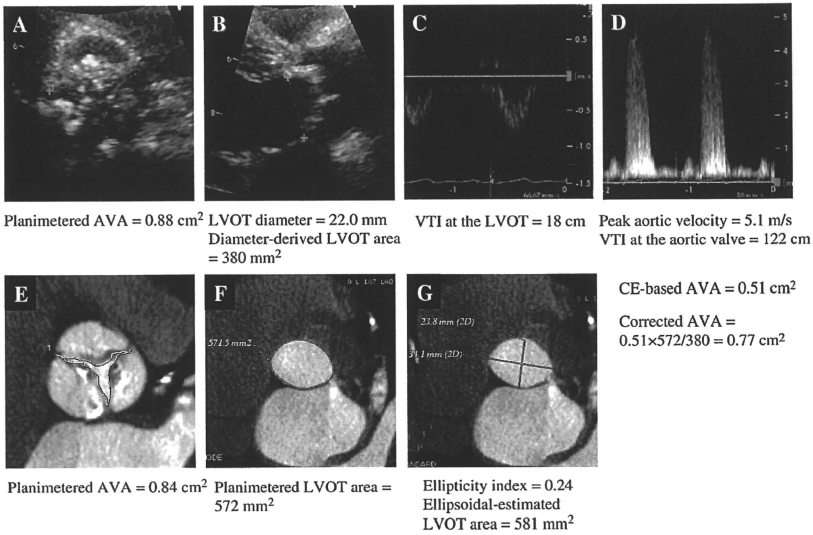

Fig. 5. The echocardiographic planimetered AVA is 0.88 cm^2 (A). The echocardiographic LVOT diameter is 22.0 mm and the diameter-derived LVOT area is calculated as 380 mm^2 (B). Doppler tracings show the velocity–time integral (VTI) at the LVOT (C) and the aortic valve (D). The CE-based AVA is calculated as 0.51 cm^2. Meanwhile, the MDCT planimetered AVA is 0.84 cm^2 (E). From a double oblique transversal image of the LVOT, the LVOT area is directly measured as 572 mm^2 (F) and the ellipsoidal-estimated LVOT area is calculated as 581 mm^2 (G). When the CE is corrected with the MDCT planimetered LVOT area, the CE-based AVA is corrected to 0.77 cm^2. The measurement error decreases from 39% to 8%. Abbreviations are as detailed in Fig. 1.

between CE-based AVA and planimetered AVA have been put forward. This discrepancy may represent the difference between the anatomic AVA (geometric orifice area) measured with planimetry and the averaged effective AVA (effective orifice area) computed using the CE [2]. The planimetered AVA indicates the maximal opening area in the systolic phase, whereas the CE-based AVA indicates the average systolic opening of the aortic valve because the VTI is a time-averaged systolic velocity [8]. If the ascending aorta is narrow, pressure recovery phenomenon distal to the stenosis can lead to a measurement error in the CE-based AVA [15,16].

In the present study, the actual cross-sectional LVOT area was underestimated using diameter-derived LVOT area calculations due to the assumption of circular geometry. Notably, the ellipticity index was larger in severe AS patients than in others, resulting in larger measurement error of CE-based AVA ranging from 20 to 39%. When the MDCT planimetered LVOT area was included in the CE, the measurement error significantly decreased in patients with severe AS more than in others. Thus, we suggest that the difference in LVOT area calculations due to the assumption of a circular or ellipsoidal geometry is one of the major causes of the discrepancy between CE-based AVA and planimetered AVA values. This finding reveals CE's weak points for assessment of AS, but has only been validated in a small number of AS patients in the previous study [6]. The present study has now clearly demonstrated the impact of LVOT ellipticity on the measurement error associated with the CE-based AVA in this setting. The application of cardiac MDCT would contribute to an advance in echocardiographic diagnosis and clinical decision making, particularly in patients with severe AS, as it frequently performs due to the necessity for pre-implantation measurements prior to TAVI.

4.3. Factors related to LVOT area and ellipticity

In the present study, the MDCT planimetered LVOT area was positively correlated with BSA and height regardless of gender. Leye et al. have shown that the LVOT diameter has a good correlation with both BSA and height, independent of gender in adult AS patients [10]. However, few data are available on the relationship between actual LVOT cross-sectional area and various morphometric parameters, such as BSA and height.

Interestingly, the ellipticity index was positively correlated with peak aortic valve velocity, LV wall thickness and LV mass index, independent of age, gender and body size. A recent study has shown that LVOT geometry is more elliptical in patients with severe AS before TAVI, with a mean ellipticity index of 0.26 [13]. After AS treatment with TAVI, LVOT geometry changed to being more circular. In view of our findings, this change may result from LV reverse remodeling with regression of LV mass.

4.4. Study limitations

Firstly, there is no true gold standard for AVA calculation in this study. However, cardiac MDCT has a superior spatial signal-to-noise ratio, as compared with echocardiography, and thus would provide more detailed information about cardiac shape, effectively acting as a "clinical gold standard". Secondly, because exposure to radiation is still high during cardiac MDCT examination [17], we do not recommend this modality as a first choice for the evaluation of AS, either initially or for serial follow-up. Echocardiography including 3D volumetric imaging remains the first choice for the assessment of AS severity. Thirdly, the limits of temporal resolution with 64-MDCT would result in inadequate visualization of the valve leaflet and the

Please cite this article as: Utsunomiya H, et al, Underestimation of aortic valve area in calcified aortic valve disease: Effects of left ventricular outflow tract ellipticity, Int J Cardiol (2011), doi:10.1016/j.ijcard.2010.12.071

LVOT in patients with rapid or irregular heart rhythms. However, in our study, we did not need to exclude any patient because of inadequate image quality.

Finally, patients with bicuspid aortic valves, sigmoid septum, and ejection fraction <50% were excluded from this study because of the confounding effect in the assessment of the severity of AS [18,19]. Furthermore, the "dimensions" of Japanese patients in this study were relatively small. Thus, larger observational studies including other ethnic group are necessary to confirm our findings.

5. Conclusions

In patients with calcified aortic valve disease including AS, CE-based calculations have generally underestimated AVA values as compared with the corresponding values obtained using MDCT planimetered AVA measurements. This discrepancy is considered to be related to the fact that LVOT geometry is actually elliptical rather than circular.

Acknowledgment

The authors of this manuscript have certified that they comply with the Principles of Ethical Publishing in the International Journal of Cardiology [20].

References

[1] Baumgartner H, Hung J, Bermejo J, et al. Echocardiographic assessment of valve stenosis: EAE/ASE recommendations for clinical practice. J Am Soc Echocardiogr 2009;22:1–23.
[2] Pouleur AC, le Polain de Waroux JB, Pasquet A, Vancraeynest D, Vanoverschelde JL, Gerber BL. Planimetric and continuity equation assessment of aortic valve area: head to head comparison between cardiac magnetic resonance and echocardiography. J Magn Reson Imaging 2007;26:1436–43.
[3] Feuchtner GM, Dichtl W, Friedrich GJ, et al. Multislice computed tomography for detection of patients with aortic valve stenosis and quantification of severity. J Am Coll Cardiol 2006;47:1410–7.
[4] Tops LF, Wood DA, Delgado V, et al. Noninvasive evaluation of the aortic root with multislice computed tomography implications for transcatheter aortic valve replacement. JACC Cardiovasc Imaging 2008;1:321–30.
[5] Doddamani S, Grushko MJ, Makaryus AN, et al. Demonstration of left ventricular outflow tract eccentricity by 64-slice multi-detector CT. Int J Cardiovasc Imaging 2009;25:175–81.
[6] Halpern EJ, Mallya R, Sewell M, Shulman M, Zwas DR. Differences in aortic valve area measured with CT planimetry and echocardiography (continuity equation) are related to divergent estimates of left ventricular outflow tract area. AJR Am J Roentgenol 2009;192:1668–73.
[7] Abbara S, Pena AJ, Maurovich-Horvat P, et al. Feasibility and optimization of aortic valve planimetry with MDCT. AJR Am J Roentgenol 2007;188:356–60.
[8] Lang RM, Bierig M, Devereux RB, et al. Recommendations for chamber quantification: a report from the American Society of Echocardiography's Guidelines and Standards Committee and the Chamber Quantification Writing Group, developed in conjunction with the European Association of Echocardiography, a branch of the European Society of Cardiology. J Am Soc Echocardiogr 2005;18:1440–63.
[9] Schiller NB, Shah PM, Crawford M, et al. Recommendations for quantitation of the left ventricle by two-dimensional echocardiography. American Society of Echocardiography Committee on Standards, Subcommittee on Quantitation of Two-Dimensional Echocardiograms. J Am Soc Echocardiogr 1989;2:358–67.
[10] Leye M, Brochet E, Lepage L, et al. Size-adjusted left ventricular outflow tract diameter reference values: a safeguard for the evaluation of the severity of aortic stenosis. J Am Soc Echocardiogr 2009;22:445–51.
[11] Corciu AI, Siciliano V, Poggianti E, Petersen C, Venneri L, Picano E. Cardiac calcification by transthoracic echocardiography in patients with known or suspected coronary artery disease. Int J Cardiol 2010;142:288–95.
[12] Mohty D, Pibarot P, Despres JP, et al. Age-related differences in the pathogenesis of calcific aortic stenosis: the potential role of resistin. Int J Cardiol 2010;142:126–32.
[13] Ng ACT, Delgado V, van der Kley F, et al. Comparison of aortic root dimensions and geometries before and after transcatheter aortic valve implantation by 2- and 3-dimensional transesophageal echocardiography and multislice computed tomography. Circ Cardiovasc Imaging 2010;3:94–102.
[14] Gilon D, Cape EG, Handschumacher MD, et al. Effect of three-dimensional valve shape on the hemodynamics of aortic stenosis: three-dimensional echocardiographic stereolithography and patient studies. J Am Coll Cardiol 2002;40:1479–86.
[15] Richardson-Lobbedez M, Ennezat PV, Marechaux S. Critical impact of pressure recovery on assessment of aortic valve stenosis. Arch Cardiovasc Dis 2009;102:669–70.
[16] Baumgartner H, Stefenelli T, Niederberger J, Schima H, Maurer G. "Overestimation" of catheter gradients by Doppler ultrasound in patients with aortic stenosis: a predictable manifestation of pressure recovery. J Am Coll Cardiol 1999;33:1655–61.
[17] Pontone G, Andreini D, Bartorelli AL, et al. Diagnostic accuracy of coronary computed tomography angiography: a comparison between prospective and retrospective electrocardiogram triggering. J Am Coll Cardiol 2009;54:346–55.
[18] Poh KK, Levine RA, Solis J, et al. Assessing aortic valve area in aortic stenosis by continuity equation: a novel approach using real-time three-dimensional echocardiography. Eur Heart J 2008;29:2526–35.
[19] Donal E, Novaro GM, Deserrano D, et al. Planimetric assessment of anatomic valve area overestimates effective orifice area in bicuspid aortic stenosis. J Am Soc Echocardiogr 2005;18:1392–8.
[20] Shewan LG, Coats AJ. Ethics in the authorship and publishing of scientific articles. Int J Cardiol 2010;144:1–2.

Please cite this article as: Utsunomiya H, et al, Underestimation of aortic valve area in calcified aortic valve disease: Effects of left ventricular outflow tract ellipticity, Int J Cardiol (2011), doi:10.1016/j.ijcard.2010.12.071

JACC: CARDIOVASCULAR IMAGING
© 2010 BY THE AMERICAN COLLEGE OF CARDIOLOGY FOUNDATION
PUBLISHED BY ELSEVIER INC.

VOL. 3, NO. 9, 2010
ISSN 1936-878X/$36.00
DOI:10.1016/j.jcmg.2010.06.014

Association Between Visceral Adipose Tissue Area and Coronary Plaque Morphology Assessed by CT Angiography

Norihiko Ohashi, MD,* Hideya Yamamoto, MD, PHD,* Jun Horiguchi, MD, PHD,† Toshiro Kitagawa, MD, PHD,* Eiji Kunita, MD,* Hiroto Utsunomiya, MD,* Toshiharu Oka, MD,* Nobuoki Kohno, MD, PHD,‡ Yasuki Kihara, MD, PHD*

Hiroshima, Japan

OBJECTIVES We sought to investigate the association between visceral adipose tissue (VAT) with the presence, extent, and characteristics of noncalcified coronary plaques (NCPs) using 64-slice computed tomography angiography (CTA).

BACKGROUND Although visceral adiposity is associated with cardiovascular events, its association with NCP burden and vulnerability is not well known.

METHODS The study population consisted of 427 patients (age 67 ± 11 years; 63% men) with proven or suspected coronary artery disease who underwent 64-slice CTA. We assessed the presence and number of NCPs for each patient. The extent of NCP was tested for the difference between high (≥2) and low (≤1) counts. We further evaluated the vulnerable characteristics of NCPs with positive remodeling (remodeling index >1.05), low CT density (≤38 HU), and the presence of adjacent spotty calcium. Plain abdominal scans were also performed to measure the VAT and subcutaneous adipose tissue area.

RESULTS A total of 260 (61%) patients had identifiable NCPs. Multivariate analyses revealed that increased VAT area (per 1 standard deviation, 58 cm^2) was significantly associated with both the presence (odds ratio [OR]: 1.68; 95% confidence interval [CI]: 1.28 to 2.22) and extent (OR: 1.31; 95% CI: 1.03 to 1.68) of NCP. Other body composition measures, including subcutaneous adipose tissue area, body mass index, and waist circumference were not significantly associated with either presence or extent of NCP. Increased VAT area was also independently associated with the presence of NCP with positive remodeling (OR: 1.71; 95% CI: 1.18 to 2.53), low CT density (OR: 1.69; 95% CI: 1.17 to 2.47), and adjacent spotty calcium (OR: 1.52; 95% CI: 1.03 to 2.27).

CONCLUSIONS Increased VAT area was significantly associated with NCP burden and vulnerable characteristics identified by CTA. Our findings may explain the excessive cardiovascular risk in patients with visceral adiposity, and support the potential role of CTA to improve risk stratification in such patients. (J Am Coll Cardiol Img 2010;3:908–17) © 2010 by the American College of Cardiology Foundation

From the *Department of Cardiovascular Medicine, Graduate School of Biomedical Sciences, Hiroshima University, Hiroshima, Japan; †Department of Clinical Radiology, Hiroshima University Hospital, Hiroshima, Japan; and ‡Molecular and Internal Medicine, Graduate School of Biomedical Sciences, Hiroshima University, Hiroshima, Japan. The authors have reported that they have no relationships to disclose.

Manuscript received June 1, 2010; revised manuscript received June 22, 2010, accepted June 25, 2010.

Obesity is widely accepted as a risk factor for coronary artery disease (CAD) (1). In particular, visceral adipose tissue (VAT) accumulation was reported to be a better predictor of metabolic abnormalities and atherosclerosis than total body fat (2,3). Recent epidemiological studies have also suggested that visceral adiposity, as evaluated by the waist-to-hip ratio (4) or computed tomography (CT) scanning (5), is more closely related to cardiovascular events than is body mass index (BMI), a crude marker of total adiposity.

See page 918

We previously reported that VAT area is associated with the presence and extent of coronary artery calcium (CAC), independently of BMI, using multidetector CT (6). Whereas the presence and extent of CAC are strongly associated with the overall atherosclerotic plaque burden, it is assumed that noncalcified coronary plaques (NCPs), which contain lipid-rich components and display positive remodeling (PR), are more prone to rupture with subsequent coronary events, according to results of intravascular ultrasound (IVUS) (7) and pathologic (8) studies.

Recent advances in cardiac CT angiography (CTA) have enabled noninvasive detection of NCPs (9–12). Moreover, we previously reported that 64-slice CTA can be used to characterize NCPs in terms of composition (e.g., predominantly fibrous vs. lipid-rich plaques), vascular remodeling, and adjacent calcium morphology. We also reported that 64-slice CTA shows good agreement with IVUS (11).

To our knowledge, very few studies have examined the association between VAT, as an entity, with NCP, particularly regarding its composition and morphology. Determining the associations between VAT area and NCP burden or vulnerable characteristics seems to be important from an etiological perspective. Therefore, in this study, we used 64-slice CTA to quantitatively and qualitatively assess coronary artery plaques to determine whether VAT area is associated with the presence, extent, and vulnerable characteristics of NCPs.

METHODS

Study patients. Between November 2006 and December 2008, we recruited 565 consecutive Japanese patients with proven or suspected CAD, who underwent 64-slice CTA for the follow-up or diagnosis of CAD at our institution. For the present study, we excluded 138 subjects with a history of percutaneous coronary intervention (n = 63) or coronary artery bypass grafting (n = 62), subjects with poor image quality because of motion artifacts or inadequate contrast concentration (n = 6), and subjects with missing information for 1 or more traditional CAD risk factors (n = 7). As a result, 427 patients (267 men and 160 women, 67 ± 11 years) were finally enrolled and included in this study. In all patients, plain cardiac and abdominal scans were performed to measure the CAC score and the VAT area. The study was approved by the hospital's ethical committee, and written informed consent was obtained from all patients.

Risk factor assessment. All patients provided details of their demographics, medical history, and medications at the clinical consultation. Patients were considered current smokers if they had smoked at least 1 cigarette a day within the previous year. Hypertension was defined as systolic blood pressure ≥140 mm Hg, diastolic blood pressure ≥90 mm Hg, or on antihypertensive therapy. Diabetes mellitus was defined by self-report, a hemoglobin A_{1c} level ≥6.5% (13), or current use of hypoglycemic agents. Hypercholesterolemia was characterized by a fasting serum low-density lipoprotein cholesterol level ≥140 mg/dl on direct measurement (14) or current use of lipid-lowering agents. Height (m) and body weight (kg) were used to calculate BMI.

ABBREVIATIONS AND ACRONYMS

ACS = acute coronary syndrome
BMI = body mass index
CAC = coronary artery calcium
CAD = coronary artery disease
CT = computed tomography
CTA = computed tomography angiography
IVUS = intravascular ultrasound
NCP = noncalcified coronary plaque
PR = positive remodeling
VAT = visceral adipose tissue

Coronary CT scan protocol and reconstruction. CT examinations were performed using a 64-slice CT scanner (LightSpeed VCT, GE Healthcare, Waukesha, Wisconsin) with a gantry rotation time of 350 ms. To avoid motion artifacts, patients with a resting heart rate ≥60 beats/min were orally administered 40 mg of metoprolol at 60 min before the CT scan. All patients received 0.3 mg of nitroglycerin sublingually just before scanning. A noncontrast-enhanced scan with prospective electrocardiographic gating was performed before CTA to measure the CAC score (sequential scan with 16 × 2.5-mm collimation; tube current, 140 mA; tube voltage, 120 kV). Following a test bolus examination to determine the start of the contrast-enhanced scan, a retrospective electrocardiogram-gated CTA was performed using a helical mode during an

JACC: CARDIOVASCULAR IMAGING, VOL. 3, NO. 9, 2010
SEPTEMBER 2010:908–17

inspiratory breath-hold (64 × 0.625-mm collimation; CT pitch factor, 0.18 to 0.24:1; tube current, 600 to 750 mA with electrocardiogram-correlated tube current modulation; tube voltage, 120 kV). A body weight–adjusted volume (0.6 to 0.7 ml/kg) of contrast material (iopamidol, 370 mg I/ml, Bayer Healthcare, Berlin, Germany) was injected over the course of 10 s, followed by a saline flush of 25 ml. The effective radiation dose was estimated based on the dose-length product and ranged from 15 to 18 mSv (11).

Image reconstruction was retrospectively gated to the electrocardiogram. Depending on the heart rate, either a half-scan (temporal window = 175 ms) or a multisegment (temporal window <175 ms) reconstruction algorithm was selected, and the optimal cardiac phase with the fewest motion artifacts was chosen individually. The reconstructed image data were transferred to a remote computer workstation for post-processing (Advantage Workstation Ver.4.2, GE Healthcare) and were analyzed using dedicated software (CardIQ, GE Healthcare).

CAC scoring. CAC score was assessed by 2 blinded and independent observers using semiautomatic software (Smartscore, version 3.5, GE Healthcare). In each patient, CAC was identified as a dense area in the coronary artery exceeding the threshold of 130 HU, and the total CAC score was calculated based on the Agatston method (15).

Evaluation of plaque characteristics. All coronary segments >2 mm in diameter were evaluated by 2 blinded and independent observers using curved multiplanar reconstructions and cross-sectional images rendered perpendicular to the vessel center line. Atherosclerotic plaques were classified as calcified or noncalcified. Calcified plaques were defined as lesions composed exclusively of structures with a CT density greater than that of the contrast-enhanced coronary lumen, or with a CT density of >130 HU assigned to the coronary artery wall in a plain image. NCPs were defined as a low-density mass >1 mm^2 in size, located within the vessel wall, and clearly distinguishable from the contrast-enhanced coronary lumen and the surrounding pericardial tissue. For the analysis of plaque characteristics, the optimal image display setting was chosen on an individual basis; in general, the window was between 700 and 1,000 HU, and the level was between 100 and 200 HU.

We further evaluated the NCP characteristics on CTA by determining the minimum CT density, the vascular remodeling index, and adjacent calcium morphology, as previously described (11). The minimum CT density was determined as the lowest density of at least 5 regions of interest (area = 1 mm^2), which were placed on each lesion in a random order. Based on our previous comparison of CTA and IVUS data (11), NCP ≤38 HU (corresponding to IVUS-identified hypoechoic plaque) was defined as a low-density plaque. We then measured the cross-sectional vessel area (mm^2) for each NCP site by manually tracing the outer vessel contour (border to low-signal epicardial fat). Vascular remodeling was assessed using the remodeling index, which was calculated by dividing the cross-sectional lesion vessel area by the proximal reference vessel area. PR was defined as remodeling index >1.05 (12). Finally, based on the methods previously described (11,16), we classified calcium deposits in or adjacent to each NCP morphologically according to their length (L) and width (W) versus the vessel diameter (VD) of the coronary artery in which the calcium was observed as follows: none, undetectable; spotty, $L < 3/2$ of VD and $W < 2/3$ of VD; long, $L \geq 3/2$ of VD and $W < 2/3$ of VD; wide, $L < 3/2$ of VD and $W \geq 2/3$ of VD; and diffuse, $L \geq 3/2$ of VD and $W \geq 2/3$ of VD.

Measurement of VAT area. In addition to cardiac scans, abdominal scans were performed at the 4th to 5th lumbar levels in the spinal position, and 12 slices at 5-mm thickness were obtained during a breath-hold after normal expiration. The adipose tissue areas and waist circumference in each subject were determined from an image taken at the level of the umbilicus using dedicated software (Virtual Place, AZE Inc., Tokyo, Japan). Subcutaneous adipose tissue was defined as extraperitoneal fat between the skin and muscles, with attenuation ranging from −150 to −50 HU. Intraperitoneal fat with the same density as the subcutaneous adipose tissue layer was defined as VAT. The adipose tissue areas were determined by automatic planimetry. Waist circumference was determined at the umbilicus level using a mobile caliper.

Statistical analysis. Categorical variables are presented as the number of patients (percentage), and continuous variables are expressed as mean ± SD or medians (interquartile range). We compared sex-specific clinical and CTA characteristics between patients divided by the median values of VAT area. Differences between patients with high and low VAT area were evaluated using chi-square tests for categorical variables and the Student *t* test or Mann-Whitney *U* test for continuous variables. The presence of plaque was assessed as a binary

outcome. The extent of NCP was defined as a dichotomous variable for high (≥2) and low (≤1) NCP counts. Stratified analyses were also performed according to the vulnerable NCP characteristics (PR, low CT density, and spotty calcium). Multivariate logistic regression analyses were performed to determine whether the association between VAT area and the presence and extent of NCP was independent of age, sex, and traditional risk factors (hypertension, hypercholesterolemia, diabetes mellitus, and current smoking). We further assessed the relationship between VAT area and the presence of vulnerable NCP characteristics using age- and sex-adjusted, and multivariate logistic regression models in a hierarchal fashion. All analyses were done using JMP 5.0.1 statistical software (SAS Institute Inc., Cary, North Carolina). A p value of <0.05 was considered statistically significant.

RESULTS

Patient characteristics. Table 1 lists the clinical characteristics of the study patients according to the median VAT area (men, 126 cm^2; women, 91 cm^2). Compared with patients with low VAT area, those with high VAT area had a higher BMI, waist circumference, and subcutaneous adipose tissue area, and a higher prevalence of hypertension, hypercholesterolemia, and diabetes mellitus, in both sexes. In addition, the triglyceride and hemoglobin A_{1c} levels were higher and the high-density lipoprotein cholesterol level was lower in patients with high VAT, in both sexes. With respect to medications, patients with high VAT area had a higher prevalence of using antihypertensive agents in men, and hypoglycemic agents in both sexes.

CTA plaque characteristics. Of 427 patients, 95 (22%) had no coronary plaques. Of the remaining 332 (78%) patients, calcified plaques alone were observed in 72 (17%) patients, and NCPs were detected in 260 (61%, 189 men) patients. A total of 576 NCPs were visualized (mean 2.2 ± 1.1 per patient), and the NCPs were localized to the left main trunk (n = 57), left anterior descending artery (n = 245), left circumflex artery (n = 103), and the right coronary artery (n = 171). Of the 427 patients, 120 (28%) had a ≥50% stenotic lesion in at least 1 coronary vessel. The number of patients with NCPs with PR (remodeling index >1.05), low CT density (≤38 HU), and adjacent spotty calcium deposits was 166 (39%), 159 (37%), and 114 (27%), respectively. Seventy-one patients (17%) had NCP with all 3 characteristics.

Table 1. Characteristics of the Study Patients With High and Low VAT Area

	Men (n = 267)		Women (n = 160)	
	High VAT (n = 133)	Low VAT (n = 134)	High VAT (n = 80)	Low VAT (n = 80)
Age, yrs	65 ± 10	64 ± 12	71 ± 10	68 ± 11
BMI, kg/m^2	25.7 ± 2.7†	22.4 ± 3.1	24.7 ± 3.4†	22.1 ± 3.4
WC, cm	95.8 ± 7.5†	84.7 ± 7.6	93.7 ± 7.7†	82.3 ± 8.4
SAT, cm^2	143 ± 53†	99 ± 46	190 ± 71†	141 ± 61
Hypertension, n (%)	92 (69)*	76 (57)	48 (60)*	35 (44)
Hypercholesterolemia, n (%)	80 (60)*	61 (46)	48 (60)*	32 (40)
Diabetes mellitus, n (%)	79 (59)†	50 (37)	41 (51)†	23 (29)
Current smoking, n (%)	73 (55)	66 (49)	13 (16)	6 (8)
Total cholesterol, mg/dl	201 ± 34	196 ± 41	203 ± 39	204 ± 51
Triglycerides, mg/dl	156 (109–231)†	111 (83–157)	146 (110–210)†	98 (75–133)
HDL cholesterol, mg/dl	48 ± 14†	59 ± 18	57 ± 16†	68 ± 17
LDL cholesterol, mg/dl	119 ± 29	114 ± 32	119 ± 35	119 ± 47
HbA_{1c}, %	6.3 ± 1.3†	5.8 ± 1.3	6.3 ± 1.2†	5.8 ± 1.2
Medications				
Antihypertensive agents, n (%)	49 (37)*	32 (24)	20 (25)	22 (28)
Lipid-lowering agents, n (%)	39 (29)	32 (24)	22 (28)	18 (23)
Hypoglycemic agents, n (%)	43 (32)*	27 (20)	28 (35)*	15 (19)

Values are expressed as number (percent), mean ± SD, or medians (interquartile range). High VAT indicates VAT area greater than the sex-specific median value (men, 126 cm^2; women, 91 cm^2), and low VAT indicates VAT area less than the median value. *$p < 0.05$; †$p < 0.01$ versus low VAT group.
BMI = body mass index; HbA1c = hemoglobin A1c; HDL = high-density lipoprotein; LDL = low-density lipoprotein; SAT = subcutaneous adipose tissue; VAT = visceral adipose tissue; WC = waist circumference.

JACC: CARDIOVASCULAR IMAGING, VOL. 3, NO. 9, 2010
SEPTEMBER 2010:908–17

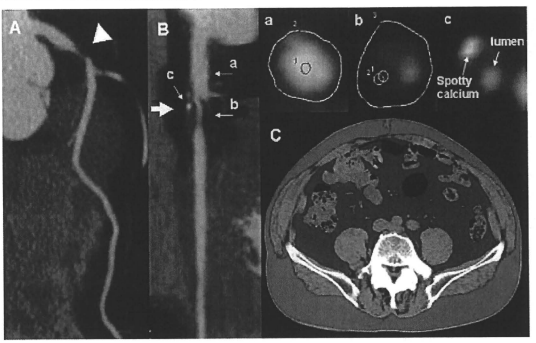

Figure 1. Coronary CT Angiography in a 74-Year-Old Man With High VAT Presenting With Unstable Angina Pectoris

(A) Shows a significant stenotic lesion in the proximal left anterior descending artery **(arrowhead)**. The stretched multiplanar reconstruction image of the vessel shows obstructive NCP with positive remodeling and adjacent spotty calcium **(B, arrow)**. The cross-sectional vessel areas of the reference site **(a)** and the lesion **(b)** are 26 and 32 mm^2, respectively. Therefore, the remodeling index is 1.23. The minimum computed tomography (CT) density of the lesion is 21 HU **(b)**. The **small circles** within the outer vessel boundaries indicate regions of interest (area = 1 mm^2) **(a, b)**. Adjacent spotty calcium can be observed in the cross-sectional image **(c)**. **(C)** Shows the abdominal adipose tissue areas at the level of the umbilicus. Regions of **blue** and **red** color indicate visceral (162 cm^2) and subcutaneous (151 cm^2) adipose tissue, respectively. CT = computed tomography; NCP = noncalcified coronary plaque; VAT = visceral adipose tissue.

Comparisons of plaque burden and vulnerable characteristics between patients with high and low VAT area. Figure 1 shows a representative CTA finding in a patient with high VAT area presenting with unstable angina pectoris. Figure 2 shows the prevalence of plaque characteristics in patients with high and low VAT area. Compared with patients with low VAT, men (71% vs. 56%, p = 0.01) and women (61% vs. 36%, p = 0.002) with high VAT were more likely to have calcified plaque. Similarly, men (82% vs. 60%, p < 0.0001) and women (56% vs. 33%, p = 0.003) with high VAT were more likely to have NCP. In analyses stratified for vulnerable NCP characteristics, patients with high

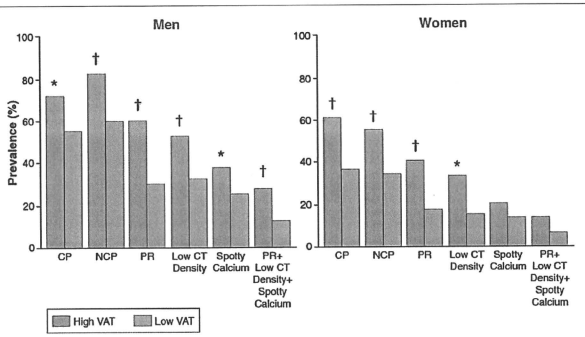

Figure 2. Prevalence of Plaque Characteristics in Patients With High and Low VAT

High VAT **(pink bars)** indicates VAT area greater than the sex-specific median value (men 126 cm^2, women 91 cm^2) and low VAT **(green bars)** indicates VAT area less than the median. CP = calcified coronary plaque; PR = positive remodeling; other abbreviations as in Figure 1. *p < 0.05; †p < 0.01.

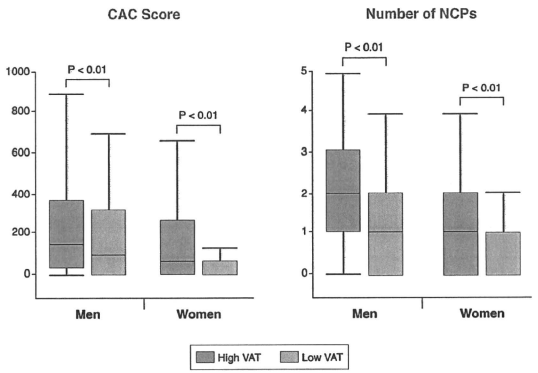

Figure 3. CAC Score and the Number of NCPs in Patients With High versus Low VAT Area

The patients with higher VAT had significantly higher median levels of CAC scores and the number of NCPs in both sexes. **Boxes** indicate 25th and 75th percentiles; **lines** indicate 5th and 95th percentiles for the data. CAC = coronary artery calcium; other abbreviations as in Figure 1.

VAT had a higher prevalence of NCP with PR (59% vs. 30%, $p < 0.0001$), low CT density (55% vs. 34%, $p = 0.0007$), and adjacent spotty calcium (41% vs. 26%, $p = 0.01$) in men, and PR (41% vs. 18%, $p = 0.001$) and low CT density (34% vs. 16%, $p = 0.01$) in women. The frequency of patients with NCP with all 3 characteristics was higher in men with high VAT (29% vs. 13%, $p = 0.001$). Figure 3 shows the CAC score and the number of NCPs for patients with high and low VAT. In both sexes, patients with high VAT area were more likely to have high CAC scores (138 [18 to 342] vs. 60 [0 to 292], $p = 0.008$ in men, 46 [0 to 246] vs. 0 [0 to 45], $p = 0.0001$ in women) and a greater extent of NCP distribution (2 [1 to 3] vs. 1 [0 to 2], $p = 0.004$ in men, 1 [0 to 2] vs. 0 [0 to 1], $p = 0.003$ in women) than those with low VAT.

Multivariate association of VAT area with calcified plaques. Calcified plaques were observed in 247 (58%, 169 men) patients. Multivariate association of VAT area with the presence of calcified plaque is presented in Table 2. As well as age, hypertension, hypercholesterolemia, and diabetes mellitus, increased VAT area was significantly associated with the presence of calcified plaque.

Multivariate associations of VAT area with NCP burden and vulnerable characteristics. Table 3 shows the association between VAT area and clinical variables with the presence and extent of NCP in all patients. In addition to age, sex, and traditional coronary risk

Table 2. Associations With the Presence of Calcified Plaque

	Univariate		Multivariate	
	OR (95% CI)*	p Value	OR (95% CI)*	p Value
Age, per 11 yrs	1.41 (1.16–1.72)	0.0006	1.60 (1.28–2.03)	<0.0001
Sex, men	1.81 (1.22–2.70)	0.003	1.56 (0.96–2.55)	0.07
VAT, per 58 cm^2	1.71 (1.37–2.15)	<0.0001	1.34 (1.05–1.73)	0.02
Hypertension	2.29 (1.55–3.41)	<0.0001	1.62 (1.05–2.50)	0.03
Hypercholesterolemia	1.73 (1.17–2.55)	0.006	1.58 (1.03–2.42)	0.04
Diabetes mellitus	2.33 (1.57–3.49)	<0.0001	2.04 (1.32–3.16)	0.001
Current smoking	1.71 (1.14–2.58)	0.01	1.44 (0.89–2.34)	0.1

*Odds ratio (95% confidence interval) for the presence of calcified plaque associated with the presence of covariates in dichotomous variables or a 1 SD increase in continuous variables.
CI = confidence interval; OR = odds ratio; other abbreviations as in Table 1.

JACC: CARDIOVASCULAR IMAGING, VOL. 3, NO. 9, 2010
SEPTEMBER 2010:908–17

Table 3. Associations With the Presence and Extent of NCP

	Presence				Extent			
	Univariate		Multivariate		Univariate		Multivariate	
	OR (95% CI)*	p Value	OR (95% CI)*	p Value	OR (95% CI)†	p Value	OR (95% CI)†	p Value
Age, per 11 yrs	1.21 (1.00–1.47)	0.05	1.45 (1.15–1.86)	0.002	1.28 (1.06–1.57)	0.01	1.53 (1.20–1.97)	0.0007
Sex, men	3.04 (2.02–4.59)	<0.0001	2.37 (1.44–3.91)	0.0007	2.42 (1.60–3.70)	<0.0001	1.85 (1.11–3.10)	0.02
VAT, per 58 cm^2	2.13 (1.71–2.82)	<0.0001	1.68 (1.28–2.22)	0.0002	1.74 (1.41–2.18)	<0.0001	1.31 (1.03–1.68)	0.03
Hypertension	2.18 (1.46–3.25)	0.0001	1.34 (0.85–2.11)	0.20	3.13 (2.08–4.79)	<0.0001	2.31 (1.46–3.68)	0.0004
Hypercholesterolemia	2.35 (1.59–3.52)	<0.0001	2.00 (1.28–3.14)	0.002	1.65 (1.12–2.44)	0.01	1.48 (0.95–2.30)	0.08
Diabetes mellitus	2.03 (1.36–3.04)	0.0005	1.61 (1.02–2.55)	0.04	2.63 (1.78–3.92)	<0.0001	2.36 (1.52–3.70)	0.0001
Current smoking	2.93 (1.91–4.57)	<0.0001	2.22 (1.33–3.74)	0.002	2.42 (1.62–3.64)	<0.0001	1.95 (1.21–3.19)	0.007

*Odds ratio (95% confidence interval) for the presence of NCP associated with the presence of covariates in dichotomous variables or a 1-SD increase in continuous variables; †odds ratio (95% confidence interval) for high NCP counts (≥2; n = 177) versus low counts (≤ 1; n = 250).
NCP = noncalcified coronary plaque; other abbreviations as in Tables 1 and 2.

factors such as hypertension, hypercholesterolemia, diabetes mellitus, and current smoking, increased VAT area (per 1 SD, 58 cm^2) was significantly associated with both the presence (odds ratio [OR]: 1.68; 95% confidence interval [CI]: 1.28 to 2.22) and extent (OR: 1.31; 95% CI: 1.03 to 1.68) of NCP. Age- and sex-adjusted Pearson's correlations between adiposity measurements are provided in Table 4. Despite the positive correlations that were found between these variables, only VAT remained an independent predictor of the presence and extent of NCP after adjustment for clinical variables (Table 5). Further adjustment for BMI, waist circumference, and subcutaneous adipose tissue area did not change the significant association of VAT with NCP (presence: OR: 1.79; 95% CI: 1.25 to 2.83, extent: OR: 1.56; 95% CI: 1.08 to 2.29). Table 6 shows the results of age- and sex-adjusted and multivariate analyses of the association between VAT and vulnerable NCP characteristics. Increased VAT area was independently associated with the presence of NCP with PR, low CT density, and adjacent spotty calcium.

DISCUSSION

In the present study, we show that VAT area is significantly associated with the presence and extent of NCP, as detected by 64-slice CTA. This association is independent of traditional coronary risk factors. Taken together with our previous reports (6), the present data indicate that visceral adiposity is associated with a higher likelihood of having CAD and, if present, more diffuse CAD compared with patients without visceral adiposity. Importantly, the study also demonstrates that high VAT area is significantly associated with the presence of NCP with PR, low CT density, and spotty calcium, which may represent vulnerable characteristics, as previously described (9,11,12). Thus, our data suggest that the accumulation of VAT may contribute to the acceleration of atherosclerosis and to plaque vulnerability.

Association between VAT area and coronary plaque burden in 64-slice CTA. We have previously reported that the accumulation of VAT is an independent predictor of the presence and extent of CAC detected by multidetector CT (6). Although several epidemiological studies have been done, there is a paucity of data regarding direct associations between VAT and the distribution of NCP. Whereas the quantification of CAC is considered to provide prognostic information (17), a recent CTA study suggested that the number of NCPs with a calcified component (namely, mixed plaques) was an independent predictor of acute cardiac events (18). In the present study, we found a positive association between VAT accumulation and NCP burden using 64-slice CTA. These findings may have important therapeutic implications because information about the plaque burden determined by CTA may help to identify patients with visceral adiposity at high risk for cardiovascular events. The identification of such patients is essential to initiate aggressive therapeutic strategies, such as lifestyle modification and pharmacological interventions.

Table 4. Age- and Sex-Adjusted Pearson's Correlation Coefficients

	VAT	SAT	BMI	WC
VAT	—			
SAT	0.53	—		
BMI	0.65	0.70	—	
WC	0.77	0.79	0.77	—

p < 0.0001 for all correlations. Abbreviations as in Table 1.

Table 5. **Associations of Adiposity Measurements With the Presence and Extent of NCP**

	Presence				Extent			
	Univariate		Multivariate*		Univariate		Multivariate*	
	OR (95% CI)†	p Value	OR (95% CI)†	p Value	OR (95% CI)‡	p Value	OR (95% CI)‡	p Value
VAT (per 58 cm^2)	2.13 (1.71–2.82)	<0.0001	1.68 (1.28–2.22)	0.0002	1.74 (1.41–2.18)	<0.0001	1.31 (1.03–1.68)	0.03
SAT (per 65 cm^2)	0.82 (0.67–1.00)	0.04	0.97 (0.77–1.23)	0.8	0.84 (0.68–1.02)	0.08	0.96 (0.75–1.22)	0.7
BMI (per 3.5 kg/m^2)	1.13 (0.94–1.37)	0.2	1.02 (0.81–1.28)	0.9	1.08 (0.89–1.32)	0.4	0.96 (0.76–1.21)	0.7
WC (per 9.6 cm)	1.37 (1.13–1.69)	0.002	1.25 (0.99–1.58)	0.06	1.23 (1.02–1.50)	0.03	1.08 (0.86–1.37)	0.5

*Adjusted for age, sex, hypertension, hypercholesterolemia, diabetes mellitus, and current smoking; †odds ratio (95% confidence interval) for the presence of NCP associated with a 1 − SD increase in adiposity measurements. ‡Odds ratio (95% confidence interval) for high NCP counts (≥2; n = 177) versus low counts (≤1; n = 250).
NCP = noncalcified coronary plaque; other abbreviations as in Tables 1 and 2.

Recent studies have suggested that increased epicardial adipose tissue (19) or low levels of adiponectin (20) are more associated with NCP rather than calcified plaque. In accordance with these results, we found that VAT had stronger association with NCP (OR: 1.68, p = 0.0002) than with calcified plaque (OR: 1.34, p = 0.02). These findings may suggest that release of inflammatory adipocytokines from VAT may sustain an active atherosclerotic process as proven by the presence of NCP. The presence of mere CAC (calcified plaque), instead, could represent a more advanced and stable phase of the atherosclerotic disease process.

The present data suggest that VAT accumulation accelerates atherosclerosis independently of traditional cardiovascular risk factors such as hypertension, hypercholesterolemia, and diabetes. These observations may contribute to our understanding that nontraditional risk factors such as hyperinsulinemia and elevated apolipoprotein B and small low-density lipoprotein particles, which are commonly found in patients with visceral adiposity, may increase the risk of CAD beyond that predicted by the presence of traditional risk factors (21). Notably, the odds ratios for NCP were higher with smoking than with VAT in a multivariate model, suggesting that smoking may facilitate the accumulation of VAT. Taking into account a previous report that smoking habits are independently related to VAT (22), smoking may confound the relationship between VAT and CAD risk.

BMI was not significantly associated with NCP in the present study. We also found that BMI and VAT area were only moderately related, indicating that BMI and VAT convey different information. Interestingly, we found that subcutaneous adipose tissue was protective against NCP in univariate analyses, which may confirm previous results that subcutaneous adiposity has favorable effects on CAD (4).

Association between VAT area and the vulnerability of NCP. Several epidemiological studies have suggested that visceral adiposity is linked to the development of acute coronary syndrome (ACS) (4,5). However, the association between visceral adiposity and coronary plaque vulnerability is unclear. Several prior CTA studies have shown that NCP is associated, more so than calcified coronary plaque, with the occurrence of ACS (9). Moreover, we previously documented that PR, low CT density, and adjacent spotty calcium represent CTA-detected plaque vulnerability (12). In the present study, using 64-slice CTA, we provide definitive evidence for increased coronary plaque vulnerability in patients with visceral adiposity.

Although there are many pathways by which visceral adiposity is causally linked to atherosclerosis, 1 possible mechanism is that adipocytokines secreted from VAT, including tumor necrosis factor-α, IL-6, free fatty acids, adiponectin, and plasminogen activator-1, may directly influence the vessel wall atherogenic environment by regulating gene expression and the function of endothelial and arterial smooth muscle, and macrophage cells (23). For example, insulin resistance, which is promoted by free fatty acids, is thought to increase atherogenesis and atherosclerotic plaque instability by inducing proinflammatory activity in vas-

Table 6. **Relationship Between VAT and NCP Characteristics in CT Angiography**

	Age- and Sex-Adjusted		Multivariate*	
	OR (95% CI)†	p Value	OR (95% CI)†	p Value
Positive remodeling	2.00 (1.57–2.57)	<0.0001	1.71 (1.18–2.53)	0.005
Low CT density	1.66 (1.33–2.11)	<0.0001	1.69 (1.17–2.47)	0.006
Spotty calcium	1.69 (1.34–2.17)	<0.0001	1.52 (1.03–2.27)	0.04
All 3 characteristics	1.89 (1.47–2.54)	<0.0001	1.58 (1.05–2.41)	0.03

*Adjusted for age, sex, BMI, SAT, WC, hypertension, hypercholesterolemia, diabetes mellitus, and current smoking; †odds ratio (95% confidence interval) for the presence of each CT characteristic per 1 − SD (58 cm^2) increase in VAT.
CT = computed tomography; NCP = noncalcified coronary plaque; other abbreviations as in Tables 1 and 2.

JACC: CARDIOVASCULAR IMAGING, VOL. 3, NO. 9, 2010
SEPTEMBER 2010:908–17

cular and immune cells (24). Furthermore, increased levels of plasminogen activator-1 can inhibit plasminogen-induced migration and proliferation of vascular smooth muscle cells, leading to the formation of plaques with thin fibrous caps, necrotic cores, and rich in macrophages that are prone to rupture (25).

Taken together, our findings may partially explain the excess cardiovascular risk in patients with visceral adiposity, suggesting that excess VAT accumulation is associated with a proinflammatory metabolic profile that is predictive of an unstable atherosclerotic plaque. Therefore, stabilization of the atherosclerotic plaque may offer a legitimate therapeutic target to reduce the risk of ACS in patients with visceral adiposity.

Study limitations. First, although our data support the notion that VAT is an important factor in the pathogenesis of atherosclerosis, causality cannot be established because this is a cross-sectional study. Prospective and larger population studies are needed to elucidate whether the occurrence of CTA-detected vulnerable NCPs, in combination with increased VAT area, might help to identify patients at high risk for cardiovascular events. Second, the study population comprised patients with proven or suspected CAD; thus, our results do not apply to patients with a lower probability of CAD. Third, inflammatory markers were not measured in the present study. The previous article (26) demonstrates that epicardial adipose tissue in patients with critical CAD has higher expressions of inflammatory mediators compared with their subcutaneous adipose tissue. Further studies are needed to clarify which inflammatory markers mediate the association between VAT and atherosclerosis. Finally, the current appropriate clinical guidelines do not recommend screening with CTA because of the high radiation exposure, the use of contrast agents, cost effectiveness and limited evidence (27). However, investigational studies using CTA should be encouraged to better understand the role of detecting the plaque burden and vulnerability in patients with visceral adiposity, which may help improve risk prediction and the prevention of such events.

CONCLUSIONS

We have demonstrated that increased VAT is significantly associated with the presence, extent, and vulnerable characteristics of NCPs, as assessed by 64-slice CTA. Our findings support the hypothesis that the accumulation of VAT may contribute to the progression and instability of coronary atherosclerotic plaques. Long-term studies of the cardiovascular event risk in patients with visceral adiposity are important, and 64-slice CTA may offer an approach to improve risk stratification in such patients.

Reprint requests and correspondence: Dr. Hideya Yamamoto, Department of Cardiovascular Medicine, Graduate School of Biomedical Sciences, Hiroshima University, 1-2-3 Kasumi Minami-ku, Hiroshima 734-8551, Japan. *E-mail: hideyayama@hiroshima-u.ac.jp.*

REFERENCES

1. Manson JE, Colditz GA, Stampfer MJ, et al. A prospective study of obesity and risk of coronary heart disease in women. N Engl J Med 1990;322:882–9.
2. Kissebah AH, Vydelingum N, Murray R, et al. Relation of body fat distribution to metabolic complications of obesity. J Clin Endocrinol Metab 1982;54:254–60.
3. Després JP, Moorjani S, Lupien PJ, Tremblay A, Nadeau A, Bouchard C. Regional distribution of body fat, plasma lipoproteins, and cardiovascular disease. Arteriosclerosis 1990;10:497–511.
4. Yusuf S, Hawken S, Ounpuu S, et al. Obesity and the risk of myocardial infarction in 27,000 participants from 52 countries: a case-control study. Lancet 2005;366:1640–9.
5. Nicklas BJ, Penninx BW, Cesari M, et al. Association of visceral adipose tissue with incident myocardial infarction in older men and women: the Health, Aging and Body Composition Study. Am J Epidemiol 2004;160:741–9.
6. Ohashi N, Yamamoto H, Horiguchi J, et al. Visceral fat accumulation as a predictor of coronary artery calcium as assessed by multislice computed tomography in Japanese patients. Atherosclerosis 2009;202:192–9.
7. Yamagishi M, Terashima M, Awano K, et al. Morphology of vulnerable coronary plaque: insights from follow-up of patients examined by intravascular ultrasound before an acute coronary syndrome. J Am Coll Cardiol 2000;35:106–11.
8. Varnava AM, Mills PG, Davies MJ. Relationship between coronary artery remodeling and plaque vulnerability. Circulation 2002;105:939–43.
9. Motoyama S, Kondo T, Sarai M, et al. Multislice computed tomographic characteristics of coronary lesions in acute coronary syndromes. J Am Coll Cardiol 2007;50:319–26.
10. Leber AW, Becker A, Knez A, et al. Accuracy of 64-slice computed tomography to classify and quantify plaque volumes in the proximal coronary system: a comparative study using intravascular ultrasound. J Am Coll Cardiol 2006;47:672–7.
11. Kitagawa T, Yamamoto H, Ohhashi N, et al. Comprehensive evaluation of non-calcified coronary plaque characteristics detected using 64-slice computed tomography in patients with proven or suspected coronary artery disease. Am Heart J 2007;154:1191–8.

12. Kitagawa T, Yamamoto H, Horiguchi J, et al. Characterization of noncalcified coronary plaques and identification of culprit lesions in patients with acute coronary syndrome by 64-slice computed tomography. J Am Coll Cardiol Cardiovasc Imaging 2009;2:153–60.
13. Nathan DM, Balkau B, Bonora E, et al. International Expert Committee report on the role of the A1C assay in the diagnosis of diabetes. Diabetes Care 2009;32:1327–34.
14. Teramoto T, Sasaki J, Ueshima H, et al. Executive summary of Japan Atherosclerosis Society (JAS) guideline for diagnosis and prevention of atherosclerotic cardiovascular diseases for Japanese. J Atheroscler Thromb 2007;14:45–50.
15. Agatston AS, Janowitz WR, Hildner FJ, et al. Quantification of coronary artery calcium using ultrafast computed tomography. J Am Coll Cardiol 1990;15:827–32.
16. Kajinami K, Seki H, Takekoshi N, Mabuchi H. Coronary calcification and coronary atherosclerosis: site by site comparative morphologic study of electron beam computed tomography and coronary angiography. J Am Coll Cardiol 1997;29:1549–56.
17. Budoff MJ, Shaw LJ, Liu ST, et al. Long-term prognosis associated with coronary calcification: observations from a registry of 25,253 patients. J Am Coll Cardiol 2007;49:1860–70.
18. Pundziute G, Schuijf JD, Jukema JW, et al. Prognostic value of multislice computed tomography coronary angiography in patients with known or suspected coronary artery disease. J Am Coll Cardiol 2007;49:62–70.
19. Alexopoulos N, McLean DS, Janik M, Arepalli CD, Stillman AE, Raggi P. Epicardial adipose tissue and coronary artery plaque characteristics. Atherosclerosis 2010;210:150–4.
20. Broedl UC, Lebherz C, Lehrke M, et al. Low adiponectin levels are an independent predictor of mixed and non-calcified coronary atherosclerotic plaques. PLoS One 2009;4:e4733.
21. Lamarche B, Tchernof A, Mauriège P, et al. Fasting insulin and apolipoprotein B levels and low-density lipoprotein particle size as risk factors for ischemic heart disease. JAMA 1998;279:1955–61.
22. Seidell JC, Cigolini M, Deslypere JP, Charzewska J, Ellsinger BM, Cruz A. Body fat distribution in relation to physical activity and smoking habits in 38-year-old European men. The European Fat Distribution Study. Am J Epidemiol 1991;133:257–65.
23. Fantuzzi G, Mazzone T. Adipose tissue and atherosclerosis: exploring the connection. Arterioscler Thromb Vasc Biol 2007;27:996–1003.
24. Kappert K, Meyborg H, Clemenz M, et al. Insulin facilitates monocyte migration: a possible link to tissue inflammation in insulin-resistance. Biochem Biophys Res Commun 2008;365:503–8.
25. Hajer GR, van Haeften TW, Visseren FL. Adipose tissue dysfunction in obesity, diabetes, and vascular diseases. Eur Heart J 2008;29:2959–71.
26. Mazurek T, Zhang L, Zalewski A, et al. Human epicardial adipose tissue is a source of inflammatory mediators. Circulation 2003;108:2460–6.
27. Bluemke DA, Achenbach S, Budoff M, et al. Noninvasive coronary artery imaging: magnetic resonance angiography and multidetector computed tomography angiography: a scientific statement from the American Heart Association Committee on cardiovascular imaging and intervention of the council on cardiovascular radiology and intervention, and the Councils on Clinical Cardiology and cardiovascular disease in the young. Circulation 2008;118:586–606.

Key Words: 64-slice computed tomography angiography ■ noncalcified coronary plaque ■ plaque vulnerability ■ visceral adipose tissue.

Journal of Digital Imaging

Is It Possible to Predict Heart Rate and Range during Enhanced Cardiac CT Scan from Previous Non-enhanced Cardiac CT?

Jun Horiguchi,[1,2,7] Hideya Yamamoto,[3] Ryuichi Arie,[4] Masao Kiguchi,[1] Chikako Fujioka,[1] Megu Ohtaki,[5] Yasuki Kihara,[3] and Kazuo Awai[6]

The effect of heart rate and variation during cardiac computed tomography (CT) on the examination quality. The purpose of this study is to investigate whether it is possible to predict heart rate and range during enhanced cardiac computed CT scan from previous non-enhanced cardiac CT scan. Electrocardiograph (ECG) files from 112 patients on three types of cardiac 64-slice CT (non-enhanced, prospective ECG-triggered and retrospective ECG-gated enhanced scans) were recorded. The mean heart rate, range (defined as difference between maximal and minimal heart rates) and the range ratio (defined as maximal heart rate divided by minimal heart rate) during the scans were compared. Scan time was 4.8, 4.6, and 7.3 s on non-enhanced, prospective ECG-triggered and retrospective ECG-gated scans, respectively ($p<0.0001$). The heart rates were not significantly different (60±9 beats per minute (bpm), 60±9 and 61±10 bpm; $p = 0.64$). Heart rate on the enhanced scan markedly correlated with that of the non-enhanced scan ($r = 0.78$ and 0.74). In contrast, the ranges of heart rate were 2±5, 4±8, and 8± 21 bpm, with different range ratios (1.04, 1.07, and 1.14; $p<0.0001$). Correlation of heart rate ranges between non-enhanced scan versus prospective ECG-triggered scan was low ($r = 0.27$) and that between non-enhanced scan versus retrospective ECG-gated scan negligible ($r = -0.027$).Heart rate on enhanced cardiac CT, in most cases, can be predicted from a non-enhanced scan. Heart rate range on enhanced cardiac CT, however, is hard to predict from the non-enhanced scan.

KEY WORDS: Cardiac, computed tomography, heart rate, heart rate range

INTRODUCTION

Image quality and detection of stenosis in coronary computed tomography (CT) angiography (CTA) is affected by heart rate and the range during acquisition.[1–6] With single-source 64-slice CTA, most investigators recommend lowering the patient's heart rate to <65 beats per minute (bpm) to achieve stable image quality.[7–10] In this range, diagnostic image quality can be obtained for all coronary arteries at a single reconstruction interval at mid-diastole.[11] When higher heart rates are included however, additional reconstructions at late systole may be required for optimal visualization of the right coronary artery.[12] The variation of heart rate alters the data acquisition window of the cardiac cycle, which may result in the inclusion of systole. In order to reduce and stabilize the heart

[1]*From the Department of Clinical Radiology, Hiroshima University Hospital, 1-2-3, Kasumi-cho, Minami-ku, Hiroshima 734-8551, Japan.*

[2]*From the Department of Radiology, Hiroshima Kyoritsu Hospital, 2-19-6, Nakasu, Asaminami-ku, Hiroshima 731-0121, Japan.*

[3]*From the Department of Cardiovascular Medicine, Hiroshima University Graduate School of Biomedical Sciences and Hiroshima University Hospital, 1-2-3, Kasumi-cho, Minami-ku, Hiroshima 734-8551, Japan.*

[4]*From the Department of Radiology, Chuden Hospital, 3-4-27, Oote-machi, Naka-ku, Hiroshima 730-8562, Japan.*

[5]*From the Department of Environmetrics and Biometrics, Research Institute for Radiation Biology and Medicine, Hiroshima University, 1-2-3, Kasumi-cho, Minami-ku, Hiroshima 734-8551, Japan.*

[6]*From the Division of Medical Intelligence and Informatics, Programs for Applied Biomedicine, Graduate School of Biomedical Sciences, Department of Radiology, Hiroshima University, 1-2-3, Kasumi-cho, Minami-ku, Hiroshima 734-8551, Japan.*

[7]*From the 2-19-6, Nakasu, Asaminami-ku, Hiroshima 731-0121, Japan.*

Correspondence to: Jun Horiguchi, 2-19-6, Nakasu, Asaminami-ku, Hiroshima 731-0121, Japan; tel: +81-82-8791111; e-mail: horiguchi@hiroshimairyo.or.jp

doi: 10.1007/s10278-010-9333-2

Published online: 08 September 2010

rate, β-blocker is often used on cardiac CT, administered orally at 1 to 2 h(s) prior to the examination or/and intravenously just before the examination.

Practitioners have to decide the acquisition protocol depending on the heart rate. electrocardiograph (ECG) editing; i.e., by arbitrarily modifying the position of the temporal windows within the cardiac cycle, to correct and compensate for part or all of the artifacts,[13] is not perfect but is the most robust imaging technique for instable heart rates. As it needs retrospective ECG-gated CTA without ECG-correlated tube current modulation however, it involves a high radiation dose. In patients with a relatively stable heart rate, ECG-correlated tube current modulation, reducing radiation exposure by 30% to 50%, is used.[14,15] In this technique, the practitioner has to determine the peak current interval relative to the cardiac phase and the minimal current value relative to the maximal current. Recently devised prospective ECG-triggered coronary 64-slice CTA[16] needs low and stable heart rate.[17]

In these circumstances, prediction of heart rate and variation is important on 64-slice CTA for deciding use of β-blockers and the determination of scanning protocol. The purpose of this study is to investigate whether it is possible to predict heart rate and range during enhanced cardiac CT from non-enhanced cardiac CT.

MATERIALS AND METHODS

Patients

The comparative study between prospective ECG-triggered and retrospective ECG-gated cardiac 64-slice CTA[18] was approved by the local hospital ethics committee and all patients provided written informed consent. This study analyzed heart rate and heart rate range of 112 patients (63 males and 49 females, 64±11 years old: ranged, 35–87 years) undergoing coronary artery calcium scoring and two types of coronary CTA. The mean body mass index was 24±13 kg/m^2. Of 112 patients, 87 (78%) were symptomatic and 71 (64%) had coronary risk factors. Using a 64-slice CT scanner (Lightspeed VCT, GE Healthcare, Waukesha, WI), 86 patients were scanned with retrospective ECG-gated CTA first, followed by prospective ECG-triggered CTA and the remaining 26 patients were scanned in reverse order. The time interval between the two scans was 5 min. To minimize motion artifacts, patients with an initial heart rate ≥60 bpm (n=83) were given with oral β-blocker (metoprolol 40 mg) to achieve a target heart rate of 50–60 bpm. No additional intravenous β-blocker, at the time of the examination, was used. Except for two patients with contraindications, nitroglycerin spray (one push, Mycor spray, Astellas pharma, Tokyo, Japan) was used 5 min before coronary CTA scan to dilate the diameters of the coronary arteries.[19]

Data Acquisition

Each scan was performed 5 s after breath-hold at mild-inspiration in order to minimize range of heart rate, which was investigated on non-enhanced cardiac CT.[20] The ECG files were obtained using three lead ECG during the CT scan, and the data were transferred to an external PC for further analysis.

The use of contrast media included 10 ml Iopamiron® 370 (Bayer-Schering Pharma, Berlin, Germany), followed by 25 ml saline chaser for test bolus scan and contrast media (volume=body weight (in kg)×0.6 ml), followed by 25 ml saline chaser for each type of coronary CTA. The injection rate of contrast media and saline was 0.06×body weight ml/s (the contrast media was administered during 10 s).

Patients with atrial fibrillation and having beat-to-beat variability exceeding 20 bpm during pre-examination baseline breathing were excluded from analysis.[21] This was because such types of heartbeat might disturb the analysis of the effect of contrast media or scan time on heart rate.

Electrocardiograph Data Evaluation and Statistical Analysis

Mean heart rate, the range (defined as difference between maximal and minimal heart rates) and the range ratio (defined as maximal heart rate divided by minimal heart rate) during scanning were compared between the three scans. Depending on the data distribution, one-factor analysis of variance (ANOVA) or Kruskal–Wallis was used.